Sensors & Actuators: B. Chemical 326 (2021) 128834

Contents lists available at ScienceDirect

Sensors and Actuators: B. Chemical

journal homepage: www.elsevier.com/locate/snb

Aliovalent Sc and Li co-doping boosts the performance of p-type NiO sensor

Junqing Chang[a,b,c], Mati Horprathum[d], Dianhui Wang[e], Gang Meng[a,c,*], Zanhong Deng[a,c], Bin Tong[a,b], Pinit Kidkhunthod[f,g], Tiantian Dai[a,b], Meng Li[a,b], Hongyu Liu[a,b], Wei Tong[h], Shimao Wang[a,c], Xiaodong Fang[a,c,i,*]

[a] *Anhui Provincial Key Laboratory of Photonic Devices and Materials, Anhui Institute of Optics and Fine Mechanics, Key Lab of Photovoltaic and Energy Conservation Materials, Hefei Institutes of Physical Science, Chinese Academy of Sciences, Hefei, 230031, China*
[b] *University of Science and Technology of China, Hefei, 230026, China*
[c] *Advanced Laser Technology Laboratory of Anhui Province, Hefei, 230037, China*
[d] *Opto-Electrochemical Sensing Research Team, National Electronic and Computer Technology Center, Pathum Thani, 12120, Thailand*
[e] *School of Materials Science and Engineering, Guilin University of Electronic Technology, Guilin, 541004, China*
[f] *Synchrotron Light Research Institute, 111 University Avenue, Muang District, Nakhon Ratchasima, 30000, Thailand*
[g] *Research Network NANOTEC-SUT on Advanced Nanomaterials and Characterization, School of Physics, Institute of Science, Suranaree University of Technology, Nakhon Ratchasima, 30000, Thailand*
[h] *Anhui Province Key Laboratory of Condensed Matter Physics at Extreme Conditions, High Magnetic Field Laboratory of the Chinese Academy of Science, Hefei, 230031, China*
[i] *College of New Materials and New Energies, Shenzhen Technology University, Shenzhen, 518118, China*

ARTICLE INFO

Keywords:
Sc and Li co-doped NiO
Nanosheet-flowers
Oxygen vacancy defect
VOCs sensing

ABSTRACT

Though p-type NiO possesses excellent catalytic oxidation property toward volatile organic compounds (VOCs), intrinsic low sensitivity of NiO (arising from the hole accumulation layer configuration in ambient air atmosphere sensor) restricts its promising applications in VOCs detection. In this study, Sc and Li were proposed to modulate the (surface) properties of NiO nanosheet-flowers based sensors. At the optimal 2 at.% Sc and 5 at.% Li doping ratio ($Ni_{0.93}Sc_{0.02}Li_{0.05}O$), the sensitivity to 100 ppm ethanol is 118.4 (105 times higher than that of pure NiO), which is comparable to or even higher than most of reported NiO based sensors. Moreover, $Ni_{0.93}Sc_{0.02}Li_{0.05}O$ sensor exhibits a low detection limit of 10 ppb, excellent repeatability and long-term stability (~30 % decline of response after 7 months). Apart from regulating the carrier concentration, defect characterizations indicate a noticeable increase of stabilized surface oxygen vacancy (O_V) defects and Ni^{3+} cations by Sc^{3+} and Li^{+} co-doping, which greatly facilitate the adsorption of VOCs molecule (revealed by density functional theory calculation) as well as the subsequent VOCs/NiO interfacial charge interaction, thus contribute to the superior sensing performances. This work demonstrates that co-doping offers an effective avenue for boosting the performances of (p-type) oxide sensors.

1. Introduction

Metal oxide semiconductor (MOS) based gas sensors have attracted great attention in the detection of volatile organic compounds (VOCs) emitted from either environment or human body, due to their small size, simple structure, all-solid state, low cost, low power consumption and easy integration [1–3]. Though p-type MOSs possess excellent catalytic oxidization properties toward VOCs molecules at moderate temperatures [4], potentially acting as excellent sensing channels with high surface reactivity, hole accumulation layer (HAL) configuration in air atmosphere suppresses their electrical responses [5]. Michael et al. reported that the gas response of p-type MOS sensors is equal to the square root of that of n-type counterparts with identical morphologies [6].

In order to address the bottleneck issue of low-response, several conceptual approaches have been proposed to trigger the surface reactivity (by introducing either intrinsic or extrinsic defects) of p-type MOSs [5]. Taking p-type binary NiO as an example, Wang et al. have reported nanostructural NiO with special morphologies, such as hollow flower-shaped microspheres, nanoscale rod-shaped flower spheres and hollow tubular structures, exhibited improved gas-sensitive properties [7–9]. Besides morphology control, catalyst loading, constructing

---

* Corresponding authors.
E-mail addresses: menggang@aiofm.ac.cn (G. Meng), xdfang@aiofm.ac.cn (X. Fang).

https://doi.org/10.1016/j.snb.2020.128834
Received 24 July 2020; Received in revised form 25 August 2020; Accepted 30 August 2020
Available online 20 September 2020

heterostructure and aliovalent cation doping have been widely applied. For example, Yu et al. [10] have synthesized Au@NiO core-shell nanoparticles, which show excellent ethanol sensing responses. Appropriate heterostructures, such as NiO-In_2O_3 and NiO-SnO_2, could also improve the (ethanol) response [11,12]. In addition, aliovalent metal cations are often introduced to the MOS lattice to form substitutional or interstitial doping, which inevitably alter the lattice parameters, carrier concentration (base resistance), surface unsaturated oxygen vacancy (O_V, widely regarded as reactive oxygen species) and other kinds of defect concentrations, providing an opportunity to activate the surface reactivity of MOS sensors [13–18]. Diverse donor dopants (Al, Fe, Sn, W, In or Ce) with higher valance sates have been proven to promote the gas response of NiO sensors [8,13,19–22]. Particularly, Fe-doped NiO hollow sphere based sensor shows the highest (100 ppm ethanol) response enhancement (31.4 times) in comparison with pure NiO hollow sphere [19]. Increase of base resistance by compensating hole carriers [16,21,23] and introduction of more surface reactive O_V defects [8,13,22,24] as a consequence of aliovalent doping have been regarded as the main reason for response enhancement. Nevertheless, surface O_V active sites sometimes are prone to be refilled by surrounding oxygen [25], especially when the sensor is operated at elevated temperatures, resulting in loss of response enhancement [26,27].

Stabilizing the surface O_V active sites has recently attracted significant attention in heterogeneous MOS catalysis [28]. Previous theoretic and experiment works indicate that lower valence state dopant, such as alkali Li, K ions, could stabilize the metastable O_V active sites in MOS [16]. In addition, Wang et al. [29] reported that Li^+ doping could induce more Ni^{3+} defects, another kind of active sites, which could greatly promote the catalytic oxidation properties of NiO. These works suggest alkali Li ion may be an appropriate dopant to further boosting the performance of high valence state ion doped NiO, with good long-term stability.

In this work, Sc^{3+} and Li^+ ions with different valence states were co-doped into the lattice of NiO. Gas sensing experiments indicate that Sc and Li co-dopant can substantially enhance the sensing performance of NiO sensor. At the optimal Li^+ ratio of 5 % and Sc^{3+} ratio of 2 %, 2 order (105 times) sensitivity enhancement (probed by 100 ppm ethanol) in comparison with pure NiO has been achieved. The Sc and Li co-doped NiO sensor also possesses low ethanol detection limit of ~ 10 ppb and excellent reproducibility. Apart from well-known base resistance (carrier) modulation, and introduction of surface O_V, addition of Li^+ dopant in Sc doped NiO can not only induce more Ni^{3+} cations and surface O_V defects (by weakening the binding strength of surface oxygen) [29], but also greatly facilitate the adsorption of VOCs molecule (evidenced by density functional theory calculation), thereby contribute to the superior sensing performance with excellent long-term stability (7 months decay 30 %). This work highlights that co-doping offers an effective avenue in boosting the performance of (p-type) MOS sensors.

2. Experimental section

2.1. Materials

All chemicals employed in this work were obtained commercially without any purification and all the solutions were conducted with deionized water. Nickel oxide hydrate ($Ni(CH_3COO)_2$•xH_2O, Alfa Aesar), scandium nitrate hydrate ($Sc(NO_3)_3$•H_2O) and lithium acetate hydrate ($Li(CH_3COO)_2$•$2H_2O$) were provided by Aladdin, sodium hydroxide (NaOH) and ethylenediamine ($H_2NCH_2CH_2NH_2$) were obtained from Sinopharm Chemical Reagent Co. Ltd. All the chemical reagents were of analytical grade.

2.2. Synthesis of $Ni_{1\text{-}x\text{-}y}Sc_xLi_yO$ nanosheet-flowers

The $Ni_{1\text{-}x\text{-}y}Sc_xLi_yO$ nanosheet-lowers were synthesized via a wet chemical method [30]. Firstly, 1.5 mL of 0.5 M $Ni(CH_3COO)_2$•xH_2O, different amounts of $Sc(NO_3)_3$•H_2O or $Li(CH_3COO)_2$•$2H_2O$ ([Sc]/([Sc]+[Ni]) = 0 %, 1 %, 3 %, 6 %, 9 % and 12 %, respectively), 0.3 mL ethylenediamine and 9 mL NaOH aqueous solution were dissolved into 20 mL of deionized water under vigorous stirring to form a homogeneous blue solution. Ten minutes later, the mixed precursor was heated in an oil bath (100 °C) for 30 min with strong magnetic agitation to form a light green precipitate, then washed several times with deionized water and absolute alcohol, and dried in oven at 70 °C for 24 h. Finally, the sample was annealed in a quartz crucible at 500 °C and maintained for 2 h (the heating rate is 1 °C/min), thereby Sc-doped samples with different ratios were obtained. After determining the optimal Sc doping ratio by gas sensing test, different proportions of Li ([Li]/([Li]+[Sc]+[Ni]) = 3%, 6%, 9%, respectively) were doped according to the same steps above, and finally the powders of Sc-Li co-doped NiO were obtained. The element atomic ratios (at%) of as-synthesized samples were examined by X-ray photoelectron spectroscopy (XPS). The detailed element ratio parameters and sample nomenclature are listed in Table 1.

Table 1
The detailed element ratio and sample nomenclature of $Ni_{1\text{-}x\text{-}y}Sc_xLi_yO$.

Nominal doping ratio	Real doping ratio	Named as
0 %	0 at%	NiO
6% Sc	1.63 at% Sc	$Ni_{0.98}Sc_{0.02}O$
6% Li	5.58 at% Li	$Ni_{0.94}Li_{0.06}O$
6% Sc+3% Li	1.62 at% Sc+4.58 at% Li	$Ni_{0.94}Sc_{0.02}Li_{0.04}O$
6% Sc+6% Li	1.75 at% Sc+5.25 at% Li	$Ni_{0.93}Sc_{0.02}Li_{0.05}O$
6% Sc+9% Li	1.79 at% Sc+6.24 at% Li	$Ni_{0.92}Sc_{0.02}Li_{0.06}O$

2.3. Characterization

A field-emission scanning electron microscope (FESEM, ZEISS SUPRA 55 V P) and a transmission electron microscope and high-resolution transmission electron microscopy (TEM and HRTEM, TECNAIG2-F30S-Twin) equipped with energy dispersive spectrometer (EDS) were used to observe the morphology of powders. The crystalline characteristics of samples were collected from the X-ray powder diffraction (XRD, Rigaku Smartlab), XRD Rietveld refinements were executed by FULLPROF software. The vibrational properties of powders were analyzed by laser Raman (HORIBA) spectrometer. Brunauer-Emmett-Teller (BET) nitrogen adsorption-desorption isotherms were measured by an ASAP2460 (Micromeritics, American). X-ray photoelectron spectroscopy (XPS) measurements were carried out in an Escalab-250Xi X-ray photoelectron spectrometer microprobe with Al $K\alpha$ source (150 W). Synchrotron-based X-ray absorption near edge structure (XANES) of Ni was collected in transmission mode at the SUT-NANOTEC-SLRI XAS beamline BL5.2, SLRI, Thailand. The electron paramagnetic resonance (EPR) spectroscopy at room temperature was taken by A300−10/12 (Bruker, Germany). All the calculations are performed within density functional theory as implemented in the Vienna Ab Initio Simulation Package (VASP) [31]. The projector augmented wave (PAW) method [32] was used to describe the interaction between electrons and cores, and the generalized gradient approximation functional of Perdew, Burke and Ernzerhof [33] was used to treat the exchange-correlation energy.

2.4. Fabrication and measurement of gas sensors

The ceramic substrates (1.5 × 1.5 × 0.25 mm^3) with two heating electrodes on the back and test electrodes on the front were used (Fig. 1a, b). NiO based slurries (mixing powders with ethanol) were coated on the ceramic substrate through a drop coating to form a sensing layer (Fig. 1b). Typical thickness of the $Ni_{1\text{-}x\text{-}y}Sc_xLi_yO$ printing layer is about 9 μm (Fig. 1c). All the sensors were aged at 220 °C (4.5 V) for one week before using. The gas sensor property tests were conducted in a

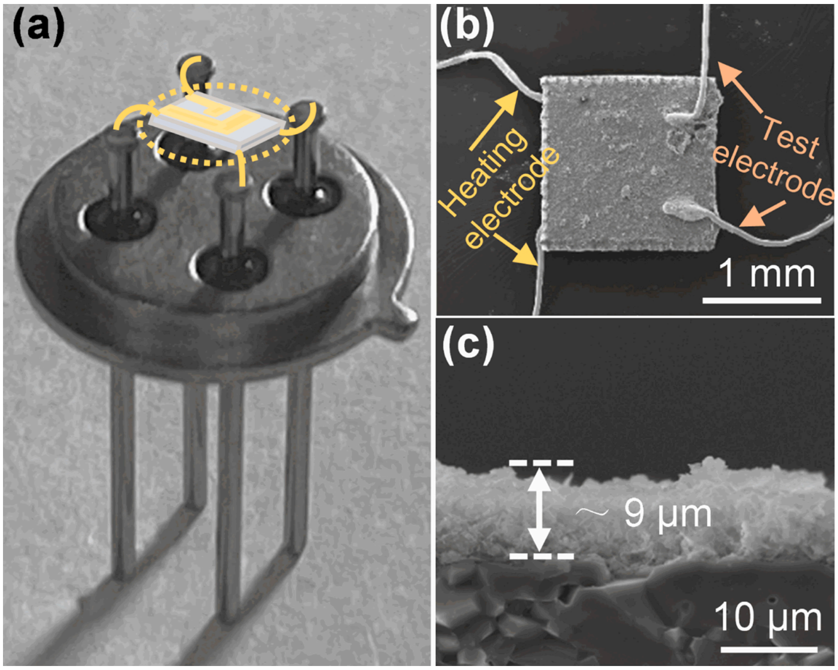

Fig. 1. NiO based sensor. (a) Schematic image. (b) SEM top view. (c) SEM cross-sectional view of the sensing layer.

four-channel gas sensor measuring system (SD101, Huachuang Ruike technology Wuhan Co. Ltd.). The working temperature was controlled by adjusting voltage bias (Fig. S1). The gas responses ($S = R_g/R_a$; R_g, resistance in gas; R_a, resistance in air) to 100 ppm ethanol, acetone, formaldehyde and H_2S were measured at 50–300 °C. With the assistance of the mass flow controller, the concentration of the target gas was adjusted by diluting the standard gas with dry air, where the total flow rate of the analytical gas and dry air was fixed at 1000 sccm.

3. Results and discussion

3.1. Characterization of sensing materials

As a starting structural basis for a variety of other nanostructures and nanocomposites prepared in this work, self-assembled nanosheet-flowers of β-$Ni(OH)_2$ were synthesized. Conversion from β-$Ni(OH)_2$ to NiO could be simply realized by sintering at 500 °C, accompanied with a slight size shrinking (Fig. S2). Morphological evolution of pure NiO and Sc, Li and Sc, Li co-doped NiO samples prepared under the same conditions was examined by SEM (Fig. 2a-d), a number of unique hierarchical flower-shape architectures with uniform size and good dispersity can be observed. Such architectures consist of many well-arranged two-dimensional thin nanosheets, and the nanosheets of nanoflowers are pretty thin and smooth, which facilitate analyte adsorption and diffusion. The averaged diameter of nano flowers decreases with Sc, Li ions doping even sharing the similar morphologies, especially for Sc and Li co-doped NiO (Fig. S3a-d). TEM (Fig. 2e) and HRTEM (Fig. 2f) were used to further analyze the structural features of $Ni_{0.93}Sc_{0.02}Li_{0.05}O$ nanosheet-flower samples. The HRTEM image exhibits clear lattice stripes with spacing of 0.239 nm, which corresponds to the (111) lattice planes of NiO. The SAED pattern reveals that Sc and Li co-doped NiO (inset of Fig. 2f) flowers adopt polycrystalline structure. The EDS analysis of Sc and Li co-doped NiO (Fig. S3e) confirms the presence of Ni, Sc and O in the samples, while Li element is tough to be detected by EDS due to quite low emitted X-ray energy (~ 55 eV). XPS (Fig. 2g-i) analysis was performed to determine the compositions of Li, Sc and co-doped NiO nanosheet-flowers, which are listed in Table 1. Fig. 2g shows the high resolution scanning of Ni $2p_{3/2}$ of pure, Sc, Li and Sc, Li co-doped NiO nanosheet-flowers, respectively. It is found that the binding energies of Ni 2*p* for these three doped NiO are higher than those of the pure NiO. It is considered that there is an orbital or electronic interaction between the extrinsic dopant and NiO matrix, because the electronegativity of Ni ($\chi = 1.91$) is higher than that of Sc ($\chi = 1.36$) and Li ($\chi = 0.98$), which eventually increases the Fermi level of NiO [34,35]. In addition, the estimated Ni^{3+}/Ni^{2+} ratios of the NiO, $Ni_{0.98}Sc_{0.02}O$, $Ni_{0.94}Li_{0.06}O$, $Ni_{0.93}Sc_{0.02}Li_{0.05}O$ specimens are 1.0, 1.4, 1.1, and 1.8, respectively. Li doping noticeably increases Ni^{3+} cations, consisting with previous report [29].

Crystal structure of pure, Sc, Li and Sc, Li co-doped NiO was examined by XRD (Fig. 3). All the diffraction peaks of all the samples can be well indexed to the face-centered cubic NiO phase (JCPDS No. 78-0423), excluding the possibility of any detectable secondary phases relevant to either Sc or Li. As both Sc^{3+} (74.5 pm) and Li^{+} (76 pm) possess a larger ionic radius than Ni^{2+} (69 pm) at the same coordination number of 6, the (substitutional) incorporation of Sc, Li causes the distortion (as well as local deformation and strain [36]) of NiO lattice, which can be confirmed by low angle shift of (220) peak (right side of Fig. 3) for Sc, Li and co-doped NiO in comparison with pure NiO. The lattice parameters of the emblematic samples were reckon from XRD and summarized in Table 2. XRD results and XRD Rietveld refinement (Fig. S4) indicate that the incorporation of Sc and Li into NiO nanosheet-flowers expands the lattice constants, which suggests a dominant substitutional doping and agrees well with the earlier reports [28,37]. The estimated average crystallite size (Table 2) of NiO, $Ni_{0.98}Sc_{0.02}O$, $Ni_{0.94}Li_{0.06}O$ and $Ni_{0.93}Sc_{0.02}Li_{0.05}O$ calculated using the Scherrer formula from XRD data is 14.8, 12.2, 17.5 and 10.3 nm, respectively. $Ni_{0.94}Li_{0.06}O$ and $Ni_{0.93}Sc_{0.02}Li_{0.05}O$ exhibit a slightly increase of lattice parameters compared to pure NiO, Meanwhile, we constructed slab model of $Ni_{0.93}Sc_{0.02}Li_{0.05}O$ with 7 atomic layers as shown in Fig. S5. The introduction of doping atoms distorted the NiO lattice. Li doping extents the grain size due to longer Li-O bond length and Sc doping shrinks the grain size (in Table S1), which consists with the experimental results. The increase of the above values can be attributed to the increase of local lattice strain caused by the increase of cation doping, thus extending the lattice, which is in line with Raman spectroscopy (Fig. S6).

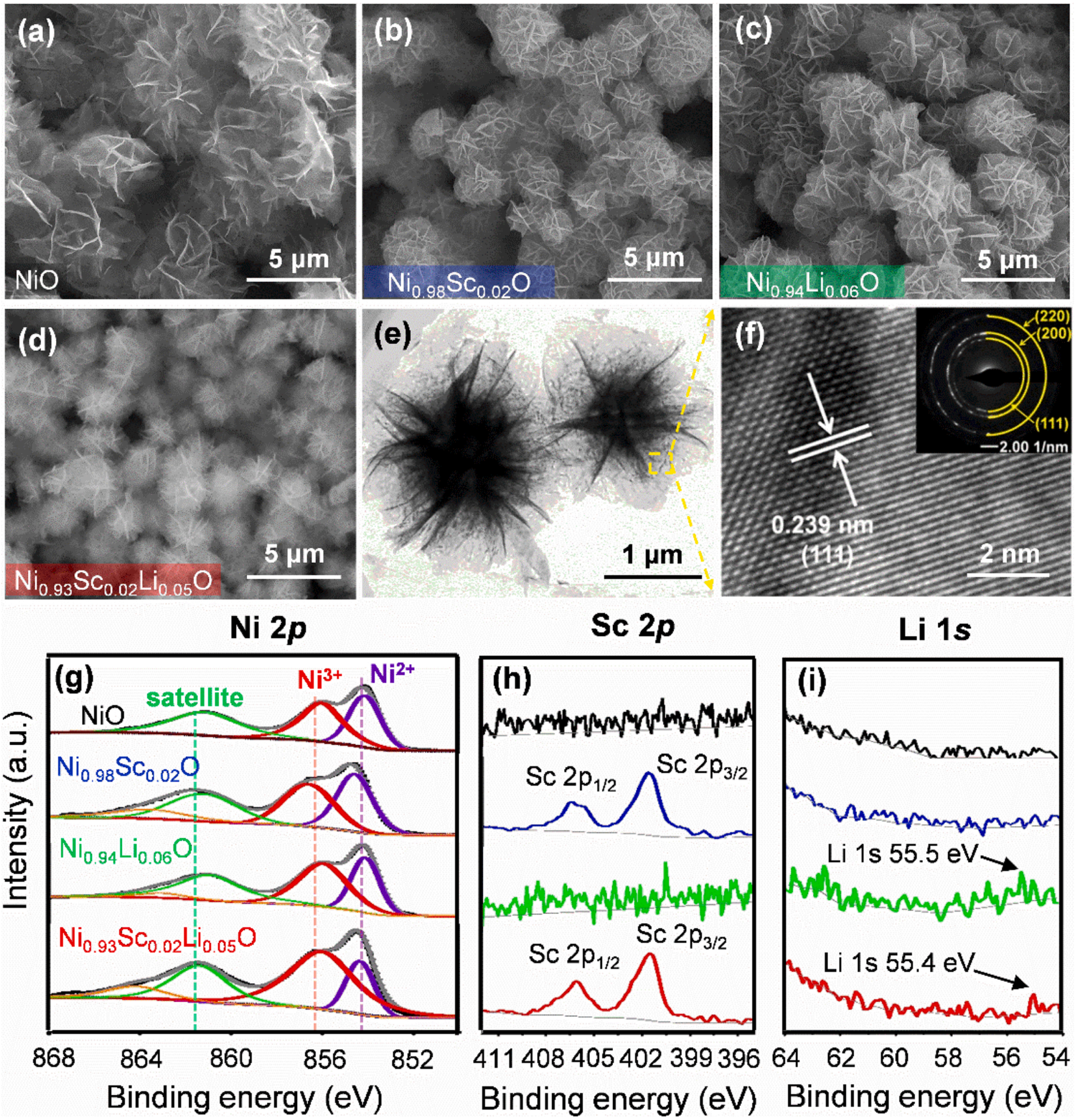

Fig. 2. SEM images of (a) NiO, (b) $Ni_{0.98}Sc_{0.02}O$, (c) $Ni_{0.94}Li_{0.06}O$ and (d) $Ni_{0.93}Sc_{0.02}Li_{0.05}O$ nanosheet-flowers. (e) TEM image and (f) HRTEM image (the inset is SAED data) of $Ni_{0.93}Sc_{0.02}Li_{0.05}O$. XPS patterns of (g) Ni 2*p*, (h) Sc 2*p* and (i) Li 1*s*.

3.2. Gas-sensing characteristics

Fig. 4 presents the sensing characteristics of four kinds of sensors (NiO, $Ni_{0.98}Sc_{0.02}O$, $Ni_{0.94}Li_{0.06}O$ and $Ni_{0.93}Sc_{0.02}Li_{0.05}O$) probed by ethanol molecules. Additional response curves of NiO doped with different ratios of Sc and Li are shown in Fig. S7. Since electrical response to VOCs arises from the charge interaction between surface reactive oxygen (ROS) and adsorbed VOCs molecules taking place at the surface active sites of the sensing material [38], appropriate thermal energy is typically required to activate these reactions. Tiny responses to 100 ppm ethanol are observed at the low operating temperature (Fig. 4a). The responses of all sensors increase rapidly with the increase of operation temperature, and decrease slightly after reaching the optimal operation temperature, exhibiting a volcanic correlation. This should be ascribed to the equilibrium between the rate of chemical reaction and the desorption of the gas [15]. The optimal operation temperature of pure NiO, $Ni_{0.98}Sc_{0.02}O$ and $Ni_{0.94}Li_{0.06}O$ is around 150 °C, while the optimal temperature of $Ni_{0.93}Sc_{0.02}Li_{0.05}O$ shifts to around 200 °C. The responses of NiO, $Ni_{0.98}Sc_{0.02}O$, $Ni_{0.94}Li_{0.06}O$ and $Ni_{0.93}Sc_{0.02}Li_{0.05}O$ to 100 ppm ethanol at 200 °C are 1.1, 6.8, 1.1 and 118.4, respectively. $Ni_{0.93}Sc_{0.02}Li_{0.05}O$ sensor displays the highest response to 100 ppm ethanol and the value is about 105 times higher than that of pure NiO, which can be clearly seen from the dynamic sensing characteristics of four sensors to 10–500 ppm ethanol at the optimal working temperature of 200 °C (Fig. 4b). $Ni_{0.93}Sc_{0.02}Li_{0.05}O$ sensor possesses a high response of 8.71 for 1 ppm ethanol and low detection limit of 10 ppb at 200 °C (Fig. 4c). The dynamic responses of four sensors versus ethanol concentrations (Fig. 4d) can be well fitted by the modified power law: $y = 1 + a\,x^b$, where y is sensor response, x is target gas concentration, a is proportional constant and b is an exponent [39]. The proportional constant is related to gas sensitivity, while the index is related to the type of pre-adsorbed ROS responsible for the

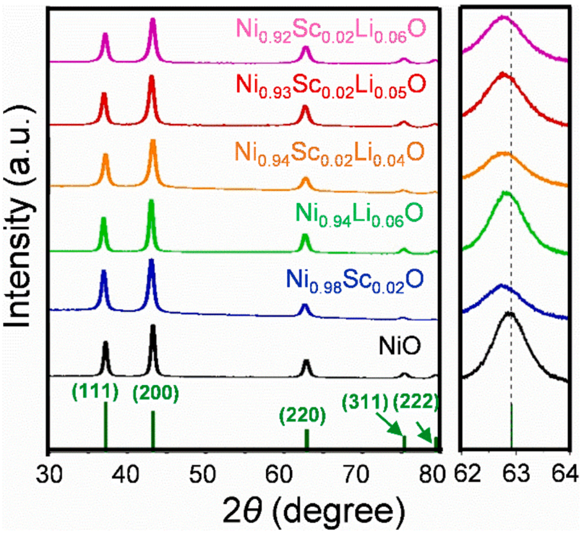

Fig. 3. XRD patterns of the pure, Li, Sc and co-doped NiO nanosheet-flowers.

Table 2
Structural parameters of NiO, $Ni_{0.98}Sc_{0.02}O$, $Ni_{0.94}Li_{0.06}O$ and $Ni_{0.93}Sc_{0.02}Li_{0.05}O$, and responses to 100 ppm ethanol at 200 °C.

Samples	Lattice constant (Å)	Averaged grain size (nm)	S_{BET} (m^2/g)	Sensitivity (R_g / R_a)
NiO	4.1781	14.8	30.3	1.1
$Ni_{0.98}Sc_{0.02}O$	4.1780	12.2	56.5	6.8
$Ni_{0.94}Li_{0.06}O$	4.1787	17.5	43.5	1.1
$Ni_{0.93}Sc_{0.02}Li_{0.05}O$	4.1822	10.3	61.4	118.4

observed gas sensing behavior. $Ni_{0.93}Sc_{0.02}Li_{0.05}O$ sensor has the highest proportional constant of 3.02, which is 173.4, 494.6 and 101.6 times higher than those of pure NiO (0.02), Sc doped NiO (0.01) and Li-doped NiO (0.03) ones, respectively, suggesting a higher surface reactivity. Meanwhile, the response increases linearly with concentration, suggesting that the active sites on the surface of $Ni_{0.93}Sc_{0.02}Li_{0.05}O$ nanosheet-flowers are not completely occupied, even when the concentration of ethanol is as high as 500 ppm [40].

Besides ethanol, acetone, formaldehyde and H_2S vapors have also been tested (Fig. 5). Despite slight variation of optimal operation temperature, $Ni_{0.93}Sc_{0.02}Li_{0.05}O$ sensor shows a drastic response enhancement for all tested vapors compared to the pure NiO. For instance, the maximal response of $Ni_{0.93}Sc_{0.02}Li_{0.05}O$ toward 100 ppm acetone at the optimal operation temperature of 220 ℃ (Fig. 5a-c) is 41.6, which is 41 times higher than that of pure NiO. Fig. 5d-f indicate that $Ni_{0.93}Sc_{0.02}Li_{0.05}O$ sensor exhibits superior formaldehyde response characteristics at 220 ℃. In addition, 51 times response enhancement to H_2S can be readily accomplished by $Ni_{0.93}Sc_{0.02}Li_{0.05}O$ sensor at 230 ℃ (Fig. 5g-i). Sc and Li co-doping not only significantly improve the sensor response, but also markedly improve the selectivity of ethanol at the optimal operating temperature of 200 °C (Fig. 6a). Principal component analysis (PCA) (Fig. 6b) indicates that four kind of tested molecules could be well separated in the three-dimensional (3D) feature space. Additional temperature dependent response data can be found in Fig. S8.

Reproducibility and (long-term) stability are critical for practical application of MOS sensors. We have monitored both short-term reproducibility (Fig. 7a-b) and long-term stability (Fig. 7c) of four devices. All sensors including $Ni_{0.93}Sc_{0.02}Li_{0.05}O$ sensor exhibit a good sensing reproducibility (Fig. 7a-b). $Ni_{0.93}Sc_{0.02}Li_{0.05}O$ sensor shows negligible decrease of response within two months, and decreases from 110 to 81 after ~ 7 months, indicating relatively good long-term stability. Degradation of response may be due to the gradual reconstruction of surface active sites on $Ni_{0.93}Sc_{0.02}Li_{0.05}O$ surface, activated by high temperature operation. Despite of that, the response of 81 is still much higher than that of undoped NiO sensor. Additional response data (Fig. S9) and relative humidity (RH) dependent ethanol responses (Fig. S10) are shown in supplementary data. Responses of NiO and $Ni_{0.93}Sc_{0.02}Li_{0.05}O$ sensor either decrease (at lower operation temperature, i.e. 200 °C) or increase (at higher operation temperature of 350 °C) with the increase of RH. Increased occupation of surface active sites by water molecules at high RH, suppressing the adsorption of ethanol molecules [41,42], results in a decrease of response at low temperature. At higher operation temperature, desorption of pre-adsorbed water molecules is noticeably speeded up. Moreover, the remaining adsorbed water molecules could react with surface O^{2-} at higher temperature, which will elevate the base resistance of NiO sensor via injecting electrons to the conduction band of NiO [43,44] and contribute to the enhancement of response. Maintaining high response in the ambient RH environment at the optimal low operation temperature is another interesting work beyond the scope of present work.

Table 3 summarizes critical parameters of NiO based sensors in the literatures and present work. Present Sc-Li co-doped NiO sensor exhibits a much higher response than most of (single cation) doped NiO based sensors, and a comparable response to Fe doped NiO sensor synergistically tailored by both (Fe) doping. and (hollow sphere) morphology control. And compared with other NiO series sensors, Sc-Li co-doped NiO sensor has a lower detection limit (~ 10 ppb) for ethanol.

3.3. Enhancement mechanism

Clarifying the underlying response enhancement mechanism is critical for the rational design of novel ultra-sensitive p-type MOS sensors with good long-term stability in future. Though we observe a decrease of averaged flower size (from 4.2 μm to 2.1 μm, Fig. S3a and Fig. S3d), grain size (from 14.8 nm to 10.3 nm, Table 2) and increase of BET surface (from 30.3 m^2/g to 61.4 m^2/g, Table 2 and Fig. S 11) by Sc and Li co-doping, slight variation of these factors may be hard to drastically improve (2 orders) sensing performance of NiO sensor. Concerning the raise of base resistance (R_a) by Sc^{3+} doping, previously regarded as the main reason for response enhancement of Fe, W and Sn doped NiO sensors [19,21,23], we could observe significant R_a increase for $Ni_{0.98}Sc_{0.02}O$ and $Ni_{0.93}Sc_{0.02}Li_{0.05}O$ sensor (Fig. S13). As Li typically acts as shallow acceptor for p-type NiO [55,56], increase of Li dopant in 2 at.% Sc doped NiO from 4 at.% to 6 at.% leads to a decrease of R_a (Fig. 8). Even $Ni_{0.94}Sc_{0.02}Li_{0.04}O$ sensor exhibits the highest base resistance, its response is less than that of $Ni_{0.93}Sc_{0.02}Li_{0.05}O$ counterpart. Therefore, present response enhancement can not be simply attributed to the resistance modulation.

It is well-known that VOCs response of the MOS sensor is mainly dependent on the redox reaction of (adsorbed) reducing VOCs molecules by surface ROS (i.e. O_2^- and O^-), which are prone to be formed at surface unsaturated V_O defect sites, and could be activated by appropriate heating process, based on the reaction Eqs. 1–4:

$$O_2(gas) \rightarrow O_2(ads) \tag{1}$$

$$O_2(ads) + e^- \rightarrow O_2^-(ads) \tag{2}$$

$$O_2^-(ads) + e^- \rightarrow 2O^-(ads) \tag{3}$$

$$C_2H_5OH(ads) + 6O^-(ads) \rightarrow 2CO_2(g) + 3H_2O(g) + 6e^- \tag{4}$$

Surface V_O defects play a vital role for sensing and catalyst of MOS. XPS analysis had been performed to analyze the chemical compositions of oxygen, including lattice oxygen (O_L at 529.5 ± 0.5 eV), oxygen vacancy (O_V at 531.2 ± 0.6 eV), and chemisorbed oxygen (O_C at 532.1 ± 0.3 eV) [26] of all sensors (Fig. 9a). The ratios of O_L, O_V and O_C for NiO, $Ni_{0.98}Sc_{0.02}O$, $Ni_{0.94}Li_{0.06}O$ and $Ni_{0.93}Sc_{0.02}Li_{0.05}O$ are 59:33:8,

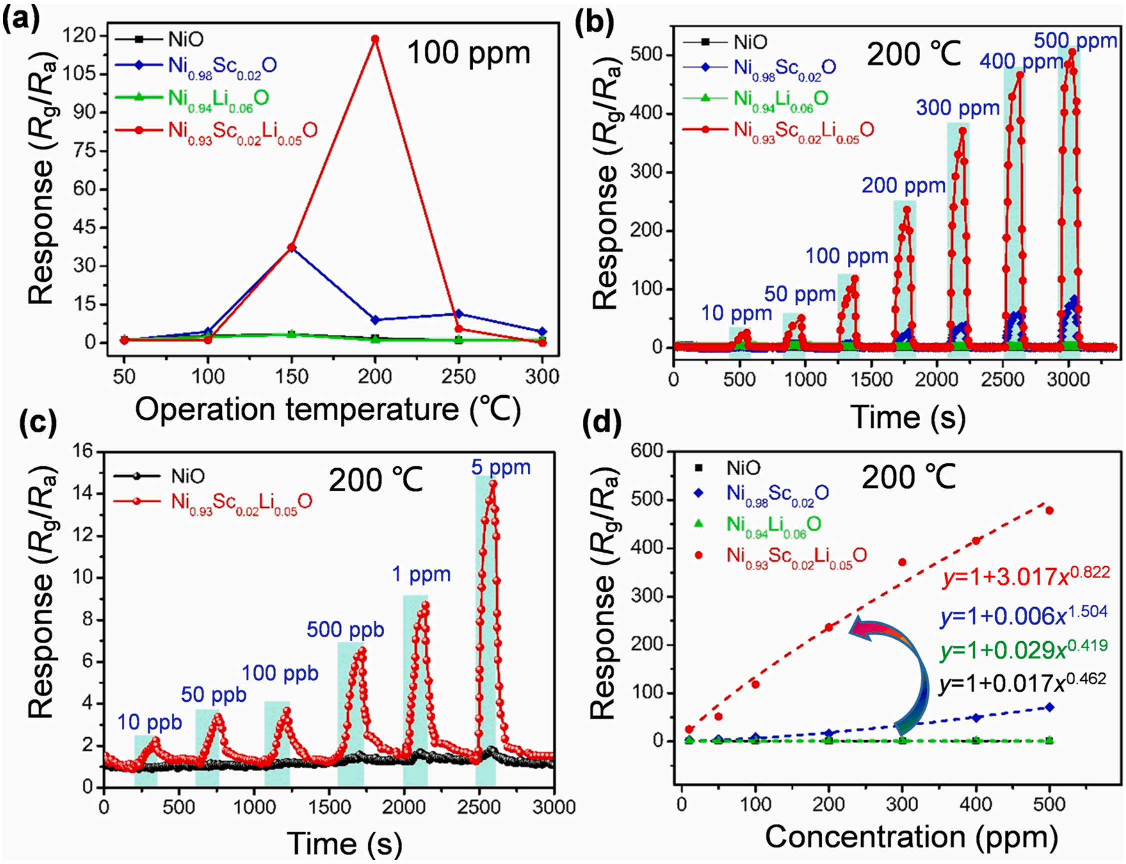

Fig. 4. (a) Responses of all sensors to 100 ppm ethanol versus the operation temperature. (b) Successive response curves of all sensors to 10-500 ppm ethanol at 200 °C. (c) Sub-ppm response and recovery curves to ethanol at 200 °C of NiO and $Ni_{0.93}Sc_{0.02}Li_{0.05}O$ sensor. (d) Concentration dependent sensitivity curves of all sensors.

55:36:9, 57:35:8 and 47:43:10, respectively. Obviously, Sc and Li co-doping increases the O_V component. In line with XPS analysis, EPR data (Fig. 9b) indicate that Sc and Li co-doped NiO sample shows the strongest (symmetric) EPR paramagnetic center signal at g = 2.003, which can be assigned to singly ionized or trapped unpaired electrons in V_O ($V_o^{\bullet}$) [57]. Besides the sharp $V_O^{\bullet}$ signal, a much boarder resonance signal with a high g value of ~ 5.8 is observed in doped NiO samples (Fig. 9c). Appearance of high *g* value resonance signal is regarded to relate with interaction between magnetic polaron and surface V_O defects [58]. High (boarder EPR signal) intensity of Sc and Li co-doped NiO infers the high surface V_O defects.

Substitutional Sc^{3+} (ionic radius of 0.745 Å) and Li^{+} (ionic radius of 0.76 Å) co-dopant may lead to large amount of NiO lattice distortion (ionic radius of Ni^{2+} 0.69 Å), inferred by Raman (Fig. S6), Rietveld refined XRD (Fig. S4) and X-ray absorption (XANES) and extended X-ray absorption fine structures (EXAFS) spectra (Fig. S12). The release of lattice distortion energy strengthened the generation of V_O, which can be expressed as formula reaction Eq. 6:

$$\frac{1}{2}O_2(g) + 2NiO \xrightarrow{2NiO} O_i^{''} \Big/ O_{surf}^{''} + 2Ni_{Ni}^{\bullet} + 2O_O^{\times} \tag{5}$$

$$O_O^{\times} \rightarrow V_O^{\bullet\bullet} + 2e^{-} + \frac{1}{2}O_2 \tag{6}$$

In comparison with single cation doping [30], the addition of Li cation can efficiently promote the performance of Sc doped NiO sensor via multiple ways: i) The incorporation of Li^{+} introduces excess holes (Fig. S13). For the charge balance, these holes can be neutralized by the neighboring Ni^{2+}, resulting in an increase of Ni^{3+} cations [29] (as revealed by XPS fitting of Ni in Fig. 2). Ni^{3+} cations possess good catalytic oxidization properties [29] and thus contribute to the electrical response. ii) It has been reported that Li dopant can weaken the binding strength of surface oxygen [59], thus noticeably promotes the surface redox reaction (4). iii) Zhan et al. has reported that the alkali metal ions can stabilize the metastable active sites [16], that is why the Sc and Li co-doped NiO sensor exhibits excellent long-term stability (Fig. 7). iv) Theoretic calculations of ethanol adsorption configuration on Sc and Li

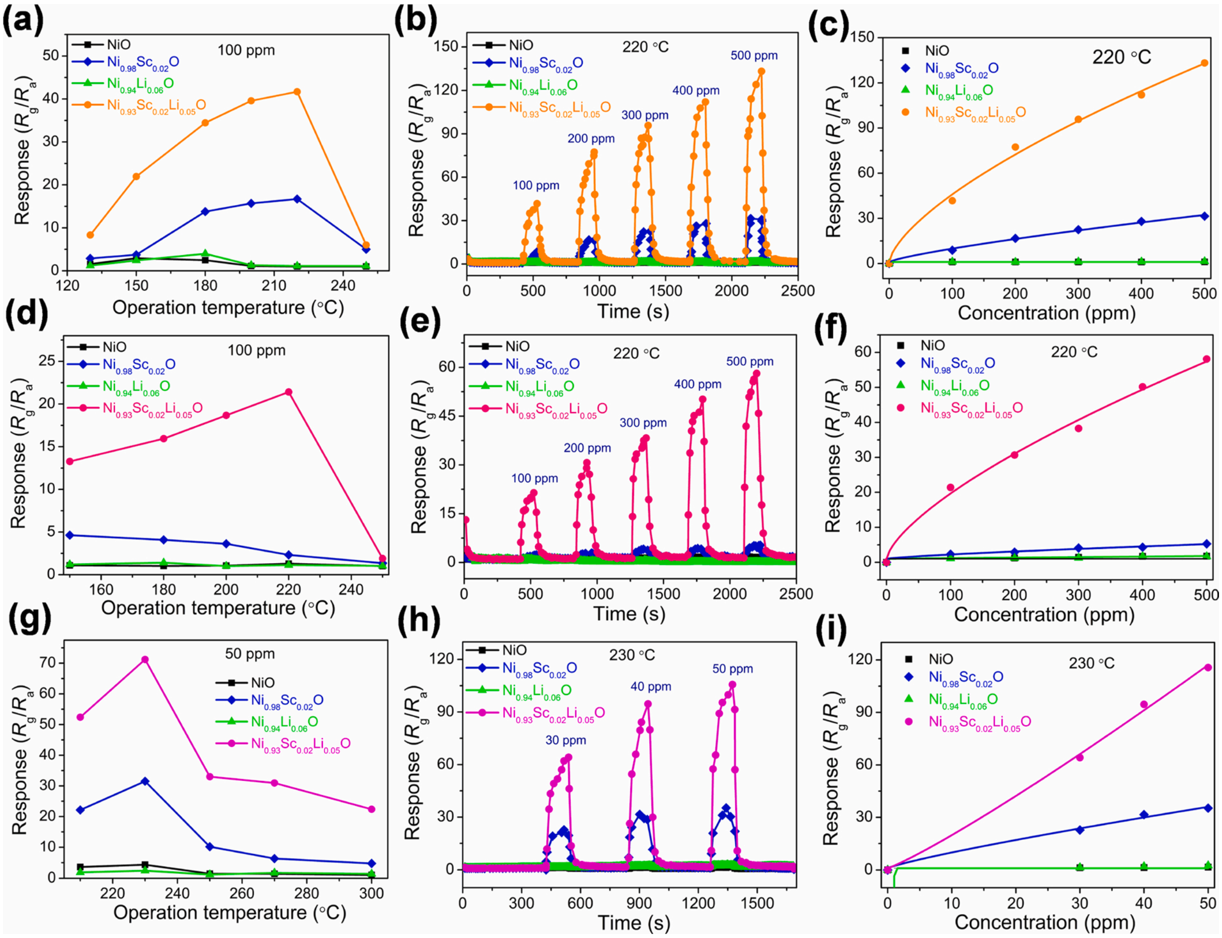

Fig. 5. Response of all sensors to (a) 100 ppm acetone, (d) 100 ppm formaldehyde and (g) 50 ppm H_2S as function of the operation temperature. Successive response curves of all sensors to (b) 100 – 500 ppm acetone at 220 ℃, (e) 100 – 500 ppm formaldehyde at 220 ℃ and 30 – 50 ppm H_2S at 230 ℃. Concentration dependent response curves of all sensors to (c) acetone, (f) formaldehyde and (i) H_2S.

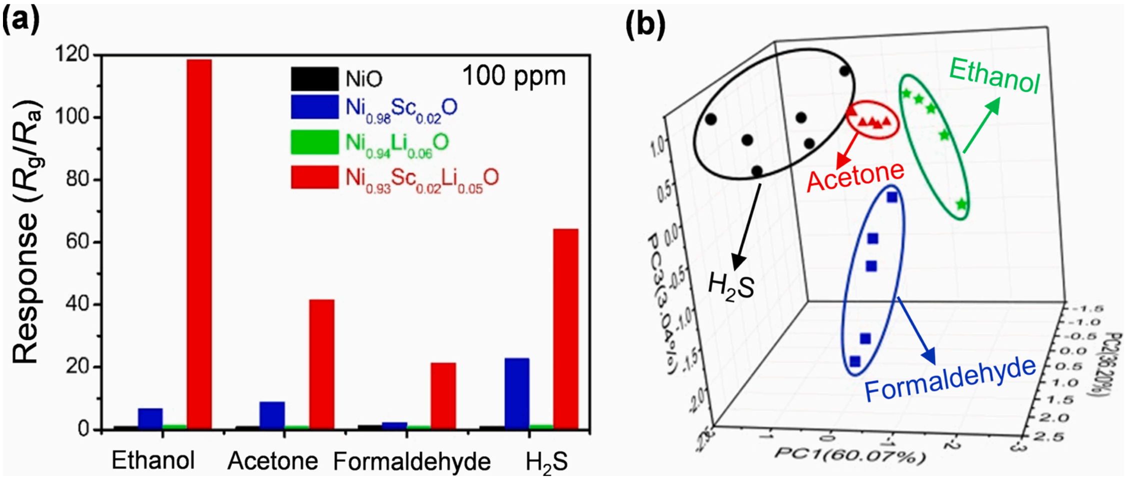

Fig. 6. (a) Response characteristics of all sensors to diverse vapors at fixed operation temperature of 200 °C. (b) PCA analysis of 4 kinds of vapors (colored online).

co-doped NiO surface (Fig. 10) indicate a preferential adsorption of ethanol molecule on Li-O bond (2.164 Å), other than Ni-O bond (2.189 Å) in Fig. 10b. More negative adsorption energy on Li sites (-1.044 eV) than Ni sites (-0.217 eV) suggests alkali Li dopants efficiently promote the adsorption of analyte molecules. On the basis of the aforementioned analysis, the introduction of Li and Sc dopant can offer abundant (stabilized) reactive sites and trigger the surface reactivity of NiO, and thus drastically improves the gas sensing performance of NiO sensor.

Fig. 11 depicts the ethanol response mechanism for NiO nanosheet-flowers based sensors. Upon exposure to air, oxygen ionosorption (capturing free electrons from the valence band of NiO), results in a low R_a (HAL) and generation of ROS O^{2-}, O^{-} species for oxidizing adsorbed ethanol molecules via reaction (4). The generated electrons were

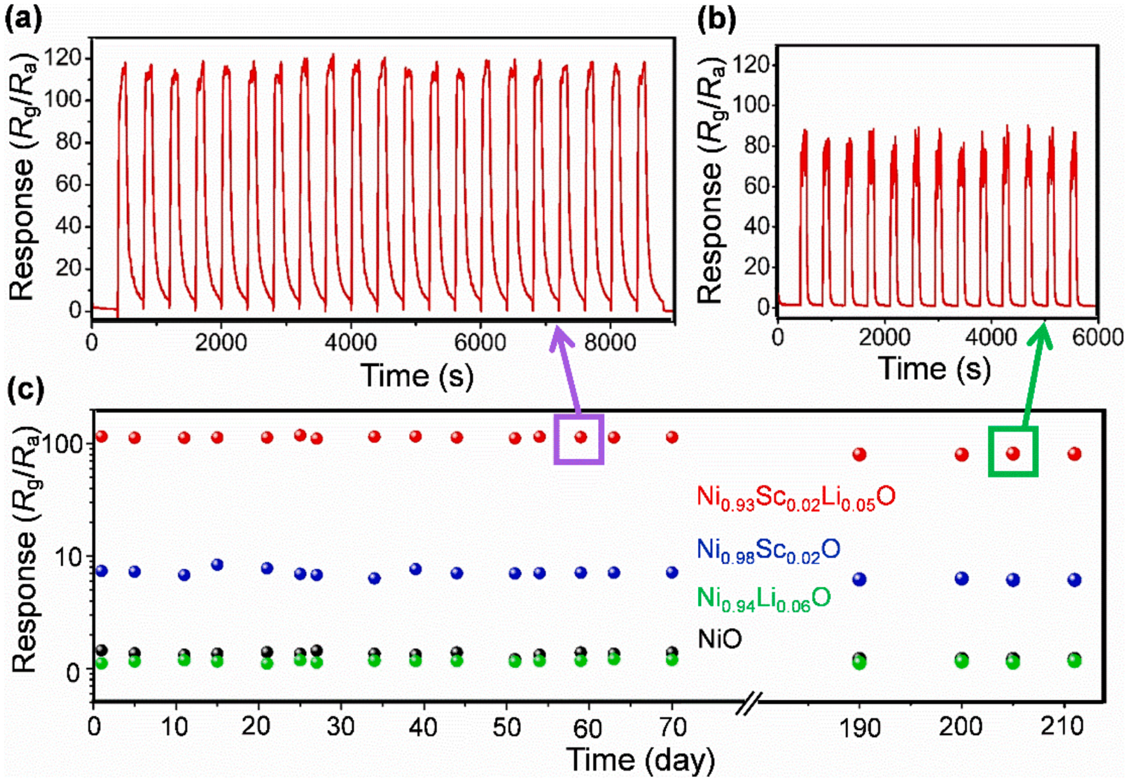

Fig. 7. (a) Repeatability of $Ni_{0.93}Sc_{0.02}Li_{0.05}O$ sensor to 100 ppm ethanol for 21 cycles after 58 days. (b) Repeatability of $Ni_{0.93}Sc_{0.02}Li_{0.05}O$ sensor to 100 ppm ethanol for 13 cycles after 190 days. (c) Long-term stability of NiO based sensors to 100 ppm ethanol.

Table 3
Sensing performance of various NiO-based sensors to VOCs between the current work and previously reported results.

Materials	Target gas	Temp. (°C)	Conc. (ppm)	S_R	τ_{res}/τ_{rec} (s)	Stability (day) / decay (%)	LOD (ppb)	Ref.
Al-doped NiO nanorod-flowers	ethanol	200	100	12.0	–	–	–	[8]
Fe-doped NiO NWs	ethanol	320	100	14.3	25 / 11	210 / 5.7	–	[19]
In-doped NiO NFs	methanol	300	200	10.9	273 / 26	30 / 20.2	–	[22]
Sn-doped NiO NWs	ethanol	340	100	15.6	19 / 24	210 / 5.1	–	[23]
Au@NiO core-shell NPs	ethanol	200	100	2.54	250 / 420	–	2000	[27]
B- and N-codoped graphene NiO NDs	H_2S	150	100	82	29 / 78	21 / 1.9	24	[28]
Fe-doped NiO microspheres	triethylamine	160	10	12.8	83 / 73	–	–	[45]
W-doped NiO NTs	xylene	375	200	8.7	178 /152	30 / ~2.7	–	[21]
Sn-doped NiO NPs	xylene	225	100	20.2	298 / 223	20 / 6.3	300	[20]
Ce-doped NiO NPs	NO_2	150	40	29.2	62 / 595	–	–	[13]
Zn-doped NiO	formaldehyde	200	1.4	~150	540 /780	–	74	[24]
Cr-doped NiO	xylene	325	50	88	144 / 50	30 / 1.0	5000	[46]
Sc-doped NiO	acetone	245	100	109.4	62 / 41	50 / 20	10	[30]
Pt/NiO thin film	NH_3	300	1000	127.8	15 / 76	–	10	[47]
CuO-NiO p-p NTs	glycol	110	100	10.35	15 /45	60 / 6.3	78	[25]
	ethanol	110	100	2.42	21 / 38	–	–	
NiO/SnO_2 p-n heterojunctions	ethanol	300	100	27.5	2.9 / 4.7	56 / 1.1	50	[12]
NiO-In_2O_3 p-n NFs	ethanol	300	100	78	86 / -	14 /-	–	[39]
NiO-RuO_2 NPs	ethanol	350	2000	35.9	35 / 124	–	~5000	[48]
NiO/SnO_2 microcubes	formaldehyde	240	100	27	5 / 15	–	130	[11]
NiO-TiO_2 NRs	acetone	400	200	9.33	8 / 480	–	–	[49]
NiO-WO3 NFs	acetone	375	100	22.5	6 / 11	20 / ~0.2	–	[50]
NiO-ZnO flower-like	acetone	300	200	38.8	3 / 41	18 / -	–	[51]
NiO-Fe_2O_3 NPs	H_2S	300	200	26.55	10 / 20	–	–	[52]
NiO-ZnO NWs	ethanol	400	50	6.7	–	–	60	[53]
	acetone	400	100	10			80	
NiO-SnO_2 MFs	formaldehyde	100	100	39.2	28 / 115	30 / ~2.5	1000	[54]
$Ni_{0.93}Sc_{0.02}Li_{0.05}O$	ethanol	200	100	118.4	86 / 31	213 / 30	10	This work

rejected into NiO, resulting in a decrease in the thickness of HAL, thereby increase the sensor resistance. Sc and Li co-dopant introduces a large number surface active sites (O_V defects and Ni^{3+} cations), which noticeably promote the adsorption and the subsequent redox reaction taking place at NiO surface.

4. Conclusion

In summary, we have demonstrated that Sc and Li co-dopant can profoundly boost the performance of NiO sensor, including 2 orders increase of response, a low detection limit of 10 ppb and 7 months

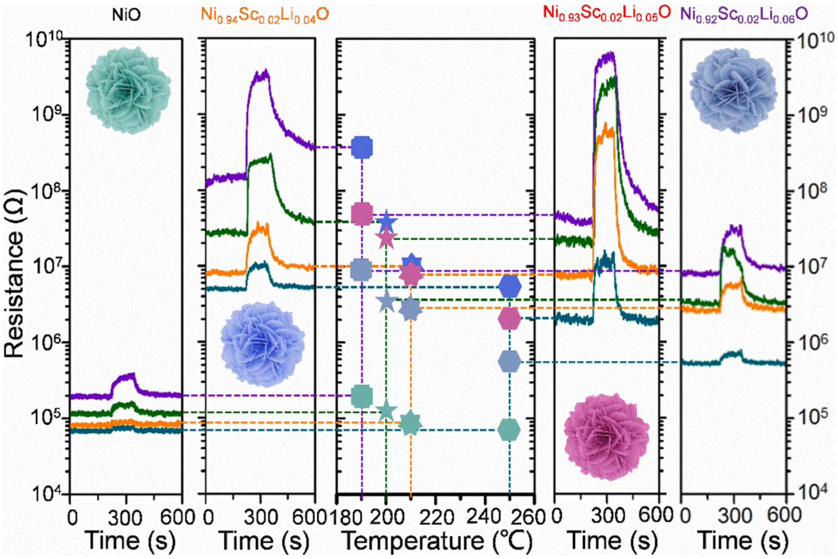

Fig. 8. Dynamic sensing transients and sensor resistances at 190 – 250 °C of NiO, $Ni_{0.94}Sc_{0.02}Li_{0.04}O$, $Ni_{0.93}Sc_{0.02}Li_{0.05}O$ and $Ni_{0.92}Sc_{0.02}Li_{0.06}O$ sensors.

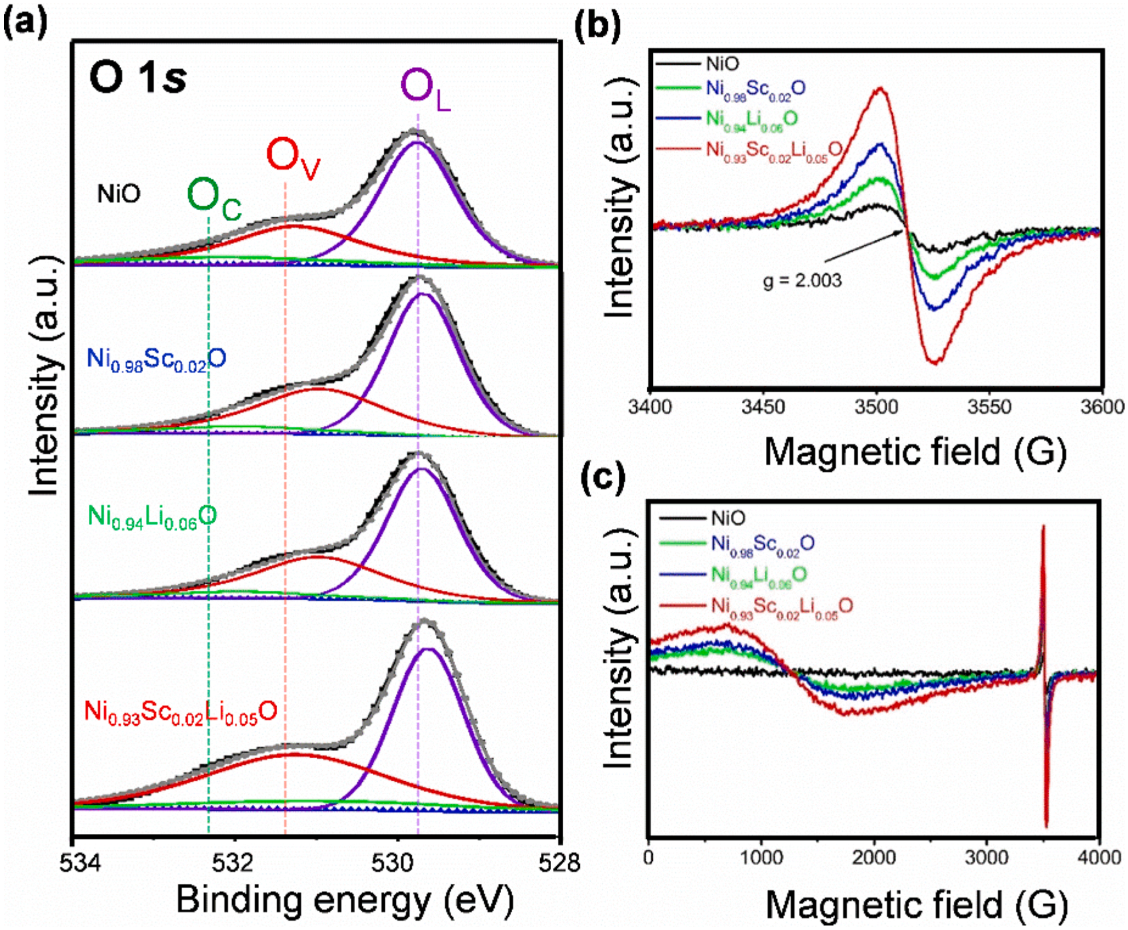

Fig. 9. (a) XPS patterns of O 1*s*, (b) room-temperature EPR range from 3250 – 3750 G, (c) room-temperature EPR range from 0 – 5000 G for four sensors.

stability (probed by ethanol molecules). Defect characterizations indicate that the incorporation of aliovalent Sc^{3+} and Li^{+} cations with large ionic radius, results in the deformation of NiO lattice and an increase of surface active sites (unsaturated V_O defects and Ni^{3+} cations). In particularly, Li cations play an important role on generation of Ni^{3+} cations, stabilize V_O defect and facilitate ethanol adsorption. This work highlights the importance of co-doping on triggering surface reactivity of MOS and offers valuable guidance for developing novel high-performance (p-type) MOS type VOCs sensors.

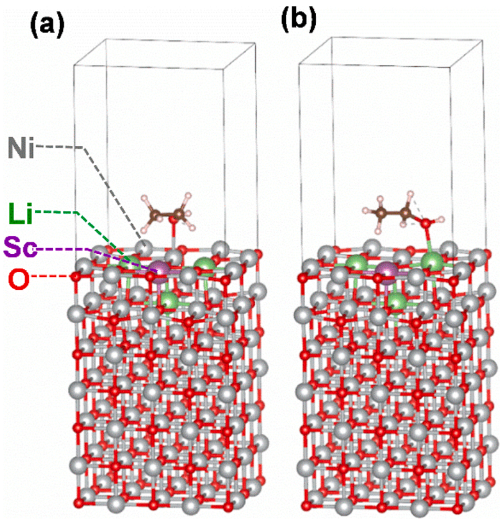

Fig. 10. Adsorption state of ethanol molecule on $Ni_{0.93}Sc_{0.02}Li_{0.05}O$ (100) surface. (a) O atom of ethanol is attached to a Ni atom; (b) O atom of ethanol is attached to a Li atom. The gray, red, green, purple, brown, and pink balls represent Ni, O, Sc, Li, C, and H atoms, respectively. (For interpretation of the references to colour in this figure legend, the reader is referred to the web version of this article).

CRediT authorship contribution statement

Junqing Chang: Methodology, Writing - original draft. **Mati Horprathum:** Formal analysis. **Dianhui Wang:** Formal analysis. **Gang Meng:** Conceptualization, Visualization, Writing - review & editing. **Zanhong Deng:** Formal analysis, Writing - review & editing. **Bin Tong:** Validation. **Pinit Kidkhunthod:** Data curation. **Tiantian Dai:** Validation. **Meng Li:** Data curation. **Hongyu Liu:** Formal analysis. **Wei Tong:** Investigation. **Shimao Wang:** Methodology. **Xiaodong Fang:** Supervision, Project administration.

Declaration of Competing Interest

The authors declare no competing financial interest.

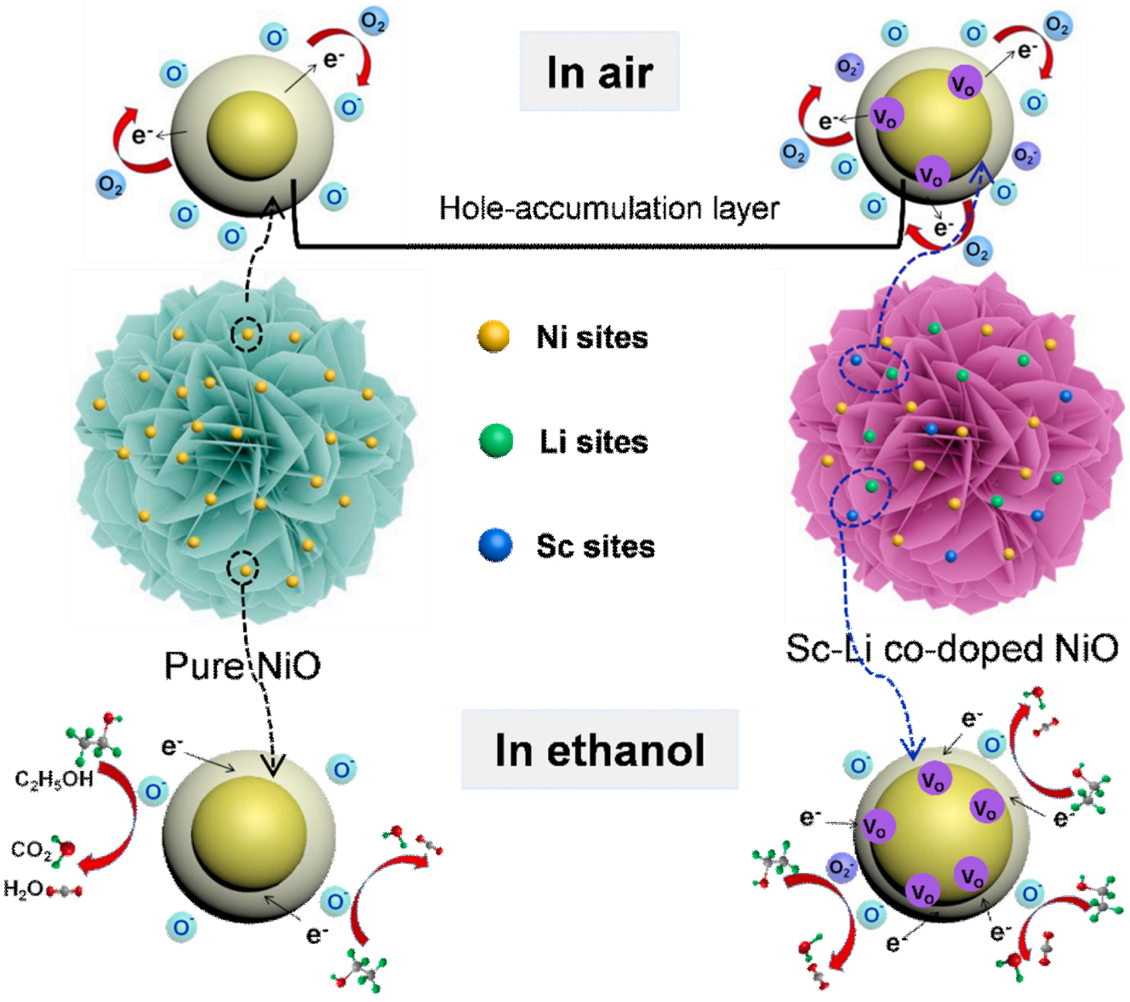

Fig. 11. Schematic illustration of sensing mechanism of pure NiO and co-doped NiO sensors.

Acknowledgments

This work was financially supported by the CAS Pioneer Hundred Talents Program of Chinese Academy of Sciences, National Natural Science Foundation of China (11604339, 11674324), CAS-NSTDA Joint Research Projects (GJHZ202101), CAS-JSPS Joint Research Projects (GJHZ1891), Natural Science Foundation of Top Talent of SZTU (2020101), National Electronics and Computer Technology Center (P2050221), National Key Laboratory of Quantum Optics and Photonic Devices (KF201901) and the Key Lab of Photovoltaic and Energy Conservation Materials (PECL2018QN001 and PECL2019QN005). Junqing Chang thanks Chuang Tian for help on XRD Rietveld refinements and Anhui Provincial Key Laboratory of Photonics Devices and Materials for partial experimental supports.

Appendix A. Supplementary data

Supplementary material related to this article can be found, in the online version, at doi:https://doi.org/10.1016/j.snb.2020.128834.

References

[1] I.-D. Kim, A. Rothschild, H.L. Tuller, Advances and new directions in gas-sensing devices, Acta Mater. 61 (2013) 974–1000.

[2] Q. Zhu, Y.M. Zhang, J. Zhang, Z.Q. Zhu, Q.J. Liu, A new and high response gas sensor for methanol using molecularly imprinted technique, Sens. Actuators B Chem. 207 (2015) 398–403.

[3] G. Korotcenkov, B.K. Cho, Engineering approaches for the improvement of conductometric gas sensor parameters, Sens. Actuators B Chem. 188 (2013) 709–728.

[4] G.M. Bai, H.X. Dai, J.G. Deng, Y.X. Liu, K.M. Ji, Porous NiO nanoflowers and nanourchins: highly active catalysts for toluene combustion, Catal. Commun. 27 (2012) 148–153.

[5] H.J. Kim, J.H. Lee, Highly sensitive and selective gas sensors using p-type oxide semiconductors: overview, Sens. Actuators B Chem. 192 (2014) 607–627.

[6] M. Hubner, C.E. Simion, A. Tomescu-Stanoiu, S. Pokhrel, N. Barsan, U. Weimar, Influence of humidity on CO sensing with p-type CuO thick film gas sensors, Sens. Actuators B Chem. 153 (2011) 347–353.

[7] C. Wang, X. Cheng, X. Zhou, P. Sun, X. Hu, K. Shimanoe, G. Lu, N. Yamazoe, Hierarchical alpha-Fe_2O_3/NiO composites with a hollow structure for a gas sensor, ACS Appl. Mater. Interfaces 6 (2014) 12031–12037.

[8] C. Wang, X.B. Cui, J.Y. Liu, X. Zhou, X.Y. Cheng, P. Sun, X.L. Hu, X.W. Li, J. Zheng, G.Y. Lu, Design of superior ethanol gas sensor based on Al-doped NiO nanorod-flowers, ACS Sens. 1 (2016) 131–136.

[9] C. Wang, T. Wang, B. Wang, X. Zhou, X. Cheng, P. Sun, J. Zheng, G. Lu, Design of alpha-Fe_2O_3 nanorods functionalized tubular NiO nanostructure for discriminating toluene molecules, Sci. Rep. 6 (2016) 26432.

[10] S.M. Majhi, G.K. Naik, H.-J. Lee, H.-G. Song, C.-R. Lee, I.-H. Lee, Y.-T. Yu, Au@NiO core-shell nanoparticles as a p-type gas sensor: novel synthesis, characterization, and their gas sensing properties with sensing mechanism, Sens. Actuators B Chem. 268 (2018) 223–231.

[11] C. Gu, Y. Cui, L. Wang, E. Sheng, J.-J. Shim, J. Huang, Synthesis of the porous NiO/SnO_2 microspheres and microcubes and their enhanced formaldehyde gas sensing performance, Sens. Actuators B Chem. 241 (2017) 298–307.

[12] Y. Wang, H. Zhang, X. Sun, Electrospun nanowebs of NiO/SnO_2 p-n heterojunctions for enhanced gas sensing, Appl. Surf. Sci. 389 (2016) 514–520.

[13] S.R. Gawali, V.L. Patil, V.G. Deonikar, S.S. Patil, D.R. Patil, P.S. Patil, J. Pant, Ce doped NiO nanoparticles as selective NO_2 gas sensor, J. Phys. Chem. Solids 114 (2018) 28–35.

[14] C. Mrabet, M. Ben Amor, A. Boukhachem, M. Amlouk, T. Manoubi, Physical properties of La-doped NiO sprayed thin films for optoelectronic and sensor applications, Ceram. Int. 42 (2016) 5963–5978.

[15] M. Hjiri, L. El Mir, S.G. Leonardi, A. Pistone, L. Mavilia, G. Neri, Al-doped ZnO for highly sensitive CO gas sensors, Sens. Actuators B Chem. 196 (2014) 413–420.

[16] Z.F. Hao, Z.R. Shen, Y. Li, H.T. Wang, L.R. Zheng, R.H. Wang, G.Q. Liu, S.H. Zhan, The role of alkali metal in-MnO_2 catalyzed ammonia-selective catalysis, Angew. Chemie Int. Ed. English 58 (19) (2019) 6351–6356.

[17] H.D. Chen, K.L. Jin, J.C. Xu, Y.B. Han, H.X. Jin, D.F. Jin, X.L. Peng, B. Hong, J. Li, Y.T. Yang, J. Gong, H.L. Ge, X.Q. Wang, High-valence cations-doped mesoporous nickel oxides nanowires: nanocasting synthesis, microstructures and improved gas-sensing performance, Sens. Actuators B Chem. 296 (2019) 126622.

[18] J. Qu, Y.R. Ge, B.Y. Zu, Y.X. Li, X.C. Dou, Transition-metal-doped p-type ZnO nanoparticle-based sensory array for instant discrimination of explosive vapors, Small 12 (2016) 1369–1377.

[19] H.J. Kim, K.I. Choi, K.M. Kim, C.W. Na, J.H. Lee, Highly sensitive C_2H_5OH sensors using Fe-doped NiO hollow spheres, Sens. Actuators B Chem. 171 (2012) 1029–1037.

[20] H.Y. Gao, D.D. Wei, P.F. Lin, C. Liu, P. Sun, K. Shimanoe, N. Yamazoe, G.Y. Lu, The design of excellent xylene gas sensor using Sn-doped NiO hierarchical nanostructure, Sens. Actuators B Chem. 253 (2017) 1152–1162.

[21] C.H. Feng, C. Wang, H. Zhang, X. Li, C. Wang, P.F. Cheng, J. Ma, P. Sun, Y. Gao, H. Zhang, Y.F. Sun, J. Zheng, G.Y. Lu, Enhanced sensitive and selective xylene sensors using W-doped NiO nanotubes, Sens. Actuators B Chem. 221 (2015) 1475–1482.

[22] C.B. Feng, X.Y. Kou, B. Chen, G.B. Qian, Y.F. Sun, G.Y. Lu, One-pot synthesis of in doped NiO nanofibers and their gas sensing properties, Sens. Actuators B Chem. 253 (2017) 584–591.

[23] J. Wei, X. Li, Y. Han, J. Xu, H. Jin, D. Jin, X. Peng, B. Hong, J. Li, Y. Yang, H. Ge, X. Wang, Highly improved ethanol gas-sensing performance of mesoporous nickel oxides nanowires with the stannum donor doping, Nanotechnology 29 (2018) 245501.

[24] R. Lontio, H.M. Fomekong, Tedjieukeng Kamta, J. Ngolui Lambi, D. Lahem, P. Eloy, M. Debliquy, A. Delcorte, A sub-ppm level formaldehyde gas sensor based on Zn-doped NiO prepared by a co-precipitation route, J. Alloys. Compd. 731 (2018) 1188–1196.

[25] A.R. Puigdollers, P. Schlexer, S. Tosoni, G. Pacchioni, Increasing Oxide Reducibility: the role of metal/oxide interfaces in the formation of oxygen vacancies, ACS Catal. 7 (2017) 6493–6513.

[26] B. Tong, Z.H. Deng, B. Xu, G. Meng, J.Z. Shao, H.Y. Liu, T.T. Dai, X.Y. Shan, W. W. Dong, S.M. Wang, S. Zhou, R.H. Tao, X.D. Fang, Oxygen vacancy defects boosted high performance p-type delafossite $CuCrO_2$ gas sensors, ACS Appl. Mater. Interfaces 10 (2018) 34727–34734.

[27] B. Tong, G. Meng, Z.H. Deng, M. Horprathum, A. Klamchuen, X.D. Fang, Surface oxygen vacancy defect engineering of p-$CuAlO_2$ via Ar&H_2 plasma treatment for enhancing VOCs sensing performances, Chem. Commun. 55 (2019) 11691–11694.

[28] J.S. Wang, J. Liu, B. Zhang, F. Cheng, Y.J. Ruan, X. Ji, K. Xu, C. Chen, L. Miao, J. J. Jiang, Stabilizing the oxygen vacancies and promoting water-oxidation kinetics in cobalt oxides by lower valence-state doping, Nano Energy 53 (2018) 144–151.

[29] X.L. Xu, L. Li, J. Huang, H. Jin, X.Z. Fang, W.M. Liu, N. Zhang, H.M. Wang, X. Wang, Engineering Ni^{3+} cations in NiO lattice at the atomic level by Li^+ doping: the roles of Ni^{3+} and oxygen species for CO oxidation, ACS Catal. 8 (2018) 8033–8045.

[30] B. Tong, G. Meng, Z. Deng, J. Gao, H. Liu, T. Dai, S. Wang, J. Shao, R. Tao, F. Kong, W. Tong, X. Luo, X. Fang, Sc-doped NiO nanoflowers sensor with rich oxygen vacancy defects for enhancing VOCs sensing performances, J. Alloys. Compd. (2020) 155760.

[31] G. Kresse, J. Furthmüller, Efficient iiterative schemes for *ab initio* total-energy calculations using a plane-wave basis set, Phys. Rev. B 54 (1996) 11169–11186.

[32] P.E. Blochl, Projector augmented-wave method, Phys. Rev. B 50 (1994) 17953–17979.

[33] J.P. Perdew, K. Burke, M. Ernzerhof, Generalized gradient approximation made simple, Phys. Rev. Lett. 77 (1996) 3865–3867.

[34] X. Sun, X. Hu, Y. Wang, R. Xiong, X. Li, J. Liu, H. Ji, X. Li, S. Cai, C. Zheng, Enhanced gas-sensing performance of Fe-doped ordered mesoporous NiO with long-range periodicity, J. Phys. Chem. C 119 (2015) 3228–3237.

[35] B.Y. Kim, J.W. Yoon, J.K. Kim, Y.C. Kang, J.H. Lee, Dual role of multiroom-structured Sn-doped NiO microspheres for ultrasensitive and highly selective detection of xylene, ACS Appl. Mater. Interfaces 10 (2018) 16605–16612.

[36] Q. Gao, Y. Dai, B. Han, W. Zhu, X. Li, C. Li, Enhanced gas-sensitivity and ferromagnetism performances by the Ni-doping induced oxygen vacancies in (Mn, Ni) codoped ZnO nanorods, Appl. Surf. Sci. 490 (2019) 178–187.

[37] S. Manna, A.K. Deb, J. Jagannath, S.K. De, Synthesis and room temperature ferromagnetism in Fe doped NiO nanorods, J. Phys. Chem. C 112 (2008) 10659–10662.

[38] A. Mirzaei, S.G. Leonardi, G. Neri, Detection of hazardous volatile organic compounds (VOCs) by metal oxide nanostructures-based gas sensors: a review, Ceram. Int. 42 (2016) 15119–15141.

[39] X. Wang, T. Wang, G. Si, Y. Li, S. Zhang, X. Deng, X. Xu, Oxygen vacancy defects engineering on Ce-doped α-Fe_2O_3 gas sensor for reducing gases, Sens. Actuators B Chem. 302 (2020) 127165.

[40] C. Yan, H. Lu, J. Gao, G. Zhu, F. Yin, Z. Yang, Q. Liu, G. Li, Synthesis of porous NiO-In_2O_3 composite nanofibers by electrospinning and their highly enhanced gas sensing properties, J. Alloys. Compd. 699 (2017) 567–574.

[41] X. Yang, Q. Yu, S. Zhang, P. Sun, H. Lu, X. Yan, F. Liu, X. Zhou, X. Liang, Y. Gao, G. Lu, Highly sensitive and selective triethylamine gas sensor based on porous SnO_2/Zn_2SnO_4 composites, Sens. Actuators B Chem. 266 (2018) 213–220.

[42] Y. Li, N. Luo, G. Sun, B. Zhang, H. Jin, L. Lin, H. Bala, J. Cao, Z. Zhang, Y. Wang, Synthesis of porous nanosheets-assembled ZnO/$ZnCo_2O_4$ hierarchical structure for TEA detection, Sens. Actuators B Chem. 287 (2019) 199–208.

[43] G. Li, X. Zhang, H. Lu, C. Yan, K. Chen, H.B. Lu, J.Z. Gao, Z.B. Yang, G.Q. Zhu, C. L. Wang, Z. He, Ethanol sensing properties and reduced sensor resistance using porous Nb_2O_5-TiO_2 n-n junction nanofibers, Sens. Actuators B Chem. 283 (2019) 602–612.

[44] H.J. Park, J. Kim, N.J. Choi, H. Song, D.S. Lee, Nonstoichiometric co-rich $ZnCo_2O_4$ hollow nanospheres for high performance formaldehyde detection at ppb levels, ACS Appl. Mater. Interfaces 8 (2016) 3233–3240.

[45] S. Bai, H. Fu, X. Shu, R. Luo, A. Chen, D. Li, C.C. Liu, NiO hierarchical hollow microspheres doped Fe to enhance triethylamine sensing properties, Mater. Lett. 210 (2018) 305–308.

[46] C. Feng, X. Kou, X. Liao, Y. Sun, G. Lu, One-dimensional Cr-doped NiO nanostructures serving as a highly sensitive gas sensor for trace xylene detection, RSC Adv. 7 (2017) 41105–41110.

[47] H.I. Chen, C.Y. Hsiao, W.C. Chen, C.H. Chang, T.C. Chou, I.P. Liu, K.W. Lin, W. C. Liu, Characteristics of a Pt/NiO thin film-based ammonia gas sensor, Sens. Actuators B Chem. 256 (2018) 962–967.
[48] V. Kruefu, A. Wisitsoraat, D. Phokharatkul, A. Tuantranont, S. Phanichphant, Enhancement of p-type gas-sensing performances of NiO nanoparticles prepared by precipitation with RuO_2 impregnation, Sens. Actuators B Chem. 236 (2016) 466–473.
[49] G.-J. Sun, H. Kheel, S. Park, S. Lee, S. Eon Park, C. Lee, Synthesis of TiO_2 nanorods decorated with NiO nanoparticles and their acetone sensing properties, Ceram. Int. 42 (1) (2016) 1063–1069.
[50] J. Zhang, H. Lu, C. Liu, C. Chen, X. Xin, Porous NiO-WO_3 heterojunction nanofibers fabricated by electrospinning with enhanced gas sensing properties, RSC Adv. 7 (2017) 40499–40509.
[51] C. Liu, B. Wang, T. Liu, P. Sun, Y. Gao, F. Liu, G. Lu, Facile synthesis and gas sensing properties of the flower-like NiO-decorated ZnO microstructures, Sens. Actuators B Chem. 235 (2016) 294–301.
[52] G.-J. Sun, H. Kheel, J.K. Lee, S. Choi, S. Lee, C. Lee, H_2S gas sensing properties of Fe_2O_3 nanoparticle-decorated NiO nanoplate sensors, Surf. Coat. Tech. 307 (2016) 1088–1095.
[53] N. Kaur, D. Zappa, M. Ferroni, N. Poli, M. Campanini, R. Negrea, E. Comini, Branch-like NiO/ZnO heterostructures for VOC sensing, Sens. Actuators B Chem. 262 (2018) 477–485.
[54] D. Meng, D. Liu, G. Wang, Y. Shen, X. San, M. Li, F. Meng, Low-temperature formaldehyde gas sensors based on NiO-SnO_2 heterojunction microflowers assembled by thin porous nanosheets, Sens. Actuators B Chem. 273 (2018) 418–428.
[55] Y.H. Choi, D.H. Kim, S.H. Hong, P-type aliovalent Li(I) or Fe(III)-doped CuO hollow spheres self-organized by cationic complex ink printing: structural and gas sensing characteristics, Sens. Actuators B Chem. 243 (2017) 262–270.
[56] G.L. Fu, X.J. Wen, S.B. Xi, Z.L. Chen, W.W. Li, J.Y. Zhang, A. Tadich, R.B. Wu, D. C. Qi, Y.H. Du, K.H.L. Zhang, Tuning the electronic structure of NiO via Li doping for the fast oxygen evolution reaction, Chem. Mater. 31 (2019) 419–428.
[57] J. Di, J.X. Xia, M.F. Chisholm, J. Zhong, C. Chen, X.Z. Cao, F. Dong, Z. Chi, H. L. Chen, Y.X. Weng, J. Xiong, S.Z. Yang, H.M. Li, Z. Liu, S. Dai, Defect-tailoring mediated electron-hole separation in single-unit-cell Bi_3O_4Br nanosheets for boosting photocatalytic hydrogen evolution and nitrogen fixation, Adv. Meter. 31 (2019) 1807576.
[58] F. Gu, C. Li, D. Han, Z. Wang, Manipulating the defect structure (V_O) of In_2O_3 nanoparticles for enhancement of formaldehyde detection, ACS Appl. Mater. Interfaces 10 (2018) 933–942.
[59] X.L. Xu, L. Li, F. Yu, H.G. Peng, X.Z. Fang, X. Wang, Mesoporous high surface area NiO synthesized with soft templates: remarkable for catalytic CH_4 deep oxidation, Mol. Catal. 441 (2017) 81–91.

Junqing Chang is a PhD student from University of Science and Technology of China (USTC). Her work mainly focuses on the defect engineering of metal oxides (heterostructures), light modulation and sensing mechanism investigations of metal oxide based gas sensors.

Mati Horprathum is a researcher of National Electronic and Computer Technology Center (NECTEC), Thailand. His research interests are glancing-angle deposition, nano-microelectronic mechanic device, surface enhance Raman spectroscopy (SERS), fabrication and characterization of nanostructures, electrochromic thin film, vacuum design and thin film characterization.

Dianhui Wang is an associate professor in the School of Materials Science and Engineering, Guilin University of Electronic Science and Technology. His research interests include the design and development of new energy materials (including hydrogen storage materials), computational materials and photocatalytic semiconductor materials.

Gang Meng is a professor of the Anhui Institute of Optics and Fine Mechanics, Chinese Academy of Sciences (CAS). He became a professor through CAS Pioneer Hundred Talents Program in 2016. His research interests involve defect control of oxide nanomaterials, thermal management of metal oxide nano-devices for achieving low power consumption and molecule discrimination.

Zanhong Deng is an associate professor of the Anhui Institute of Optics and Fine Mechanics, CAS. Her research interests include properties tailoring and applications of p-type delafossite metal oxides.

Xiaodong Fang is a professor of the Anhui Institute of Optics and Fine Mechanics, CAS. He became a research professor of the Hundred-Talent Program from CAS in 2004. His current research interests include semiconductor nanomaterials, devices and advanced laser technologies.